

Foundations of the Quad Array of Isolating Lenses (QuAIL) Project

Katherine Golden
York University

To my cats Simon and Lily, who kept me sane through the past two years, as well as to Anna, without whom this project would never have gotten this far.

Abstract

This paper describes the QuAIL project and the steps that have been taken to lay the project's foundation. The Dragonfly Telephoto Array, an array of Canon EF 400 mm $f/2.8$ L IS II USM super-telephoto lenses coupled each to CCD cameras, opened the door to ultra-low surface brightness observations and inspired the creation of QuAIL. Building off the Dragonfly design, QuAIL will be made from an array of two to four of these super-telephoto Canon lenses which, unlike Dragonfly, will be used with extremely narrow-band interference filters. By using narrow-band filters, QuAIL will be able to isolate specific spectral lines of a target, in the process suppressing light from other wavelengths – especially from the night sky itself. In this way QuAIL will be able to look for spectral evidence indicating how dwarf spheroidal galaxies (dSphs) may have come to have such low levels of gas. QuAIL will initially use 1.0 nm wide H α filters to look for ionized hydrogen around or near dSphs. The autoguiding system for QuAIL has been developed and filters to fit the unique $f/2.8$ beam profile have been designed. Lists of potential targets to be observed in the spring and fall have also been compiled. The QuAIL project is now ready to move forward to the next stage: modifying Dragonfly's imaging array control code for use with QuAIL and beginning observations on campus.

1 Introduction

The very-low surface brightness universe is one which astronomers have barely begun to explore. Malin 1, a very-low surface brightness spiral galaxy, was the first of its kind to be discovered in 1987 (Boissier et al. 2016). With a disk surface brightness of $25.7 \text{ mag/arcsec}^2$, Malin 1 is far dimmer than the $\sim 18 \text{ mag/arcsec}^2$ surface brightness of Toronto's sky (Boissier et al. 2016; Skiff 1996). In fact, at $\sim 22 \text{ mag/arcsec}^2$, even the best possible dark sky sites have a higher sky brightness than Malin 1 (Skiff 1996). Since the discovery of this first low surface brightness spiral, thousands more low surface brightness galaxies have been discovered using various techniques to observe past the bright veil of the night sky (Boissier et al. 2016). Using the Dragonfly Telephoto Array, van Dokkum et al. (2015) discovered 47 low surface brightness objects, with central surface brightnesses ranging from $24\text{-}26 \text{ mag/arcsec}^2$, around the Coma cluster. However, until recently, it has still been very difficult to image objects with surface brightnesses fainter than $\sim 28 \text{ mag/arcsec}^2$, meaning that countless more low surface brightness objects have been out of reach of modern astronomers (Abraham & van Dokkum 2013).

For the purposes of their paper, Ivkovich and McCall (2019) defined 'dwarf' galaxies to be pressure-supported galaxies with velocity dispersions of around $\pm 30 \text{ km/s}$ or less. Adopting this definition, dwarf galaxies can be further divided into gas-rich dwarfs, such as dwarf irregular galaxies (dIs) and blue compact dwarfs (BCDs), and gas-poor dwarfs, such as dwarf spheroidal galaxies (dSphs) and dwarf elliptical galaxies (dEs) (Ivkovich & McCall 2019). Both types of

gas-rich dwarfs have surface brightness profiles which get exponentially dimmer at large radii, but towards their centers the profiles of dIs flatten while those of BCDs tend to continue to brighten (Ivkovich & McCall 2019). The dimmer of the gas-poor dwarfs, dSphs, have surface brightness profiles very similar to those of dIs while dEs have steeply rising surface brightness profiles towards their centers with the profiles decreasing roughly exponentially at large radii, like BCDs (Ivkovich & McCall 2019). The similarities in structure between dSphs (dEs) and dIs (BCDs) lead Ivkovich and McCall (2019) to believe it possible that dSphs and/or dEs are dIs and/or BCDs which have lost gas. Ivkovich and McCall (2019) refer to dIs and BCDs as late-type dwarfs (LTDs) and dSphs and dEs as early-type dwarfs (ETDs).

Dwarf spheroidal galaxies are characterized by low surface brightness, very low gas content, and generally low mass (Kirby et al. 2013). The current popular belief is that such galaxies previously possessed significantly higher concentrations of gas, similar to the concentrations of gas in dI galaxies, and that some process has removed a large portion of their gas and thus halted the galaxies' star formation (Kirby et al. 2013). The process, or combination of processes, responsible for this gas depletion has yet to be ascertained (Read & Gilmore 2005). Many processes have been proposed to explain the gas loss in dSph galaxies; some of the more popular theories are ram pressure stripping, tidal stripping, photoionization, and supernovae explosions (Read & Gilmore 2005; Ivkovich & McCall 2019).

As a galaxy moves through an intra-cluster medium or the gaseous halo of a large galaxy it experiences a sort of 'wind' which, if the wind is strong enough or the galaxy's gravitational potential well is small enough, can remove gas from the galaxy in a process called 'ram pressure stripping.' If a small galaxy is near enough to a sufficiently large galaxy then the tidal forces caused by the larger galaxy can strip materials, such as gas, away from the smaller galaxy. If ram pressure stripping or tidal effects were responsible for gas loss from a galaxy one would expect to find neutral gas around the galaxy. No such gas, however, has been found around the dSphs in the Local Group (Ivkovich & McCall 2019).

Ivkovich and McCall (2019) have suggested that low mass galaxies may have lost fast moving gas due to their small gravitational potentials, possibly by photoionization or supernovae-driven winds. Galaxies with a gravitational potential low enough to lose gas through photoionization are expected to have an absolute magnitude dimmer than approximately -16.5 in

K (Ivkoich & McCall 2019). According to Ivkoich and McCall (2019), the V-K colour of such galaxies should be about 2.5 so their absolute V magnitudes would have to be dimmer than approximately -14.0. Such galaxies should also have a B-V of 0.6 so absolute magnitude cutoff would become -13.4 in B (McCall 2018). Both photoionization and supernova shock fronts should leave traces of ionized gas in and around a galaxy.

Studying dSphs is difficult due to their very low surface brightnesses: when a galaxy produces such little light there simply isn't enough light that can be captured by conventional observing techniques to form a sufficient image of the galaxy. In recent years, proposals for how to observe ultra-low surface brightness objects have emerged and begun to be tested, including ways to collect more light and to look at only certain isolated wavelengths at a time. To collect more light from a point target the usual route would be to increase the aperture of the system. However, observing faint extended structures like dSph galaxies requires a smaller focal ratio, i.e. a faster system (Abraham & van Dokkum 2013). When observing faint extended sources, the focal ratio is more important than the aperture because the rate of photons detected per pixel of the imaging camera is inversely proportional to the focal ratio squared so the rate of photons detected per pixel can be increased by reducing the focal ratio (Abraham & van Dokkum 2013). By using filters which allow only a narrow band of wavelengths through, one is able to separate emission at a discrete wavelength from the background. A longer exposure normally admits more light from the night sky, such as city light pollution or light from the Milky Way, to pollute the image but with a narrow-band filter this undesired light can be largely excluded.

To try and tackle the issue of observing low surface brightness objects, Roberto Abraham of the University of Toronto and Pieter van Dokkum of Yale University led the development of the Dragonfly Telephoto Array. The Dragonfly team built an array of initially eight, but subsequently increased to 48, Canon EF 400 mm $f/2.8$ L IS II USM super-telephoto lenses with each lens coupled to a CCD camera (Abraham & van Dokkum 2013). By using an array of lenses one can increase the lens speed; adding additional lenses increases the aperture area, thus increasing the effective diameter without affecting the focal length (Abraham & van Dokkum 2013). In this way it is thus possible to construct an array that has an effective lens speed much faster than is physically possible with a single telescope. An added benefit of this design is the absence of diffraction spikes such as those caused by the vanes which hold up the secondary

mirrors in reflecting telescopes (Abraham & van Dokkum 2013). Using an array of eight lenses, Dragonfly was able to achieve an optical system similar to that of an $f/1.0$ refractor with a 0.4 m aperture and a $2.6^\circ \times 1.9^\circ$ field of view (Abraham & van Dokkum 2013). With their eight-lens array, the Dragonfly group has been able to easily observe targets with surface brightness levels well below 30 mag/arcsec^2 (Abraham & van Dokkum 2013).

The QuAIL project looks to take the ultra-low surface brightness viewing capabilities of the Dragonfly array one step further by incorporating ultra-narrow-band filters. The QuAIL array, initially consisting of just two super-telephoto lenses but with the option to add another two lenses later, is mounted on the side of York University's 60 cm telescope. The 60 cm telescope will act as the viewfinder and autoguiding scope for the QuAIL array, allowing longer and more stable exposures to be taken. Using narrow band $H\alpha$ filters, QuAIL will be used to search for spectral evidence indicating how dSph galaxies lost their gas. The $H\alpha$ filters will aid in the search for ionized hydrogen but in the future other filters, such as those which isolate for [O I] $\lambda 636.4 \text{ nm}$, may be used to look for the spectral lines associated with supernovae shockwaves.

By constructing an array of two lenses, one lens can be equipped with a filter for the spectral line of interest while the other lens is equipped with a continuum filter. In this way, one is able to determine the flux contributed by the continuum using the continuum filter and subtract this from the flux measured through the narrow-band filter. In an array of four lenses there are two options: a) equip two of the lenses with different narrow-band line filters and each of the other two with a corresponding continuum filter close to their wavelength or b) equip three of the lenses with identical narrow-band line filters and only one with a continuum filter. By collecting light from two different lines and using their corresponding continuum filters to subtract off the continuum, one can obtain a ratio of the signal measured for each of the two lines. By using three identical line filters and one continuum filter, one can triple the amount of signal from a signal line in the same length exposure.

2 Hardware

The initial setup of the QuAIL array consists of two Canon super-telephoto lenses secured inside custom-made lens cages. Each lens is attached to a CCD camera via a focus ring which controls the focus of the lens electronically. The CCDs and focus rings are connected to a Mac Mini computer which runs the code to control them.

2.1 Lenses

The lenses used for this project are Canon EF 400 mm $f/2.8$ L IS II USM telephoto lenses (Figure 1 below). The interior surface of these lenses have antireflection nano-structure coatings to greatly reduce the amount of scattered light within the optical system. With an aperture of 142.9 mm and a focal length of 400 mm, each lens on its own has a very fast $f/2.8$ focal ratio. By using multiple lenses to observe the same target at once, one can increase the effective aperture without affecting the focal length, thus achieving a focal ratio far faster (by the square root of the number of lenses) than physically possible with a conventional telescope system.



Figure 1: Canon EF 400 mm $f/2.8$ L IS II USM telephoto lens (Carnathan 2011).

2.2 Focusers

The focus rings used for this project were designed by Birger Engineering to work as an adapter to connect Canon EF 400 mm lenses to Diffraction Limited (formerly SBIG) CCD cameras (Figure 2 below). Besides their purpose as an adapter, these focus rings act as a spacer to bring the focal plane of the lens onto the CCD chip as well as to provide an electrical

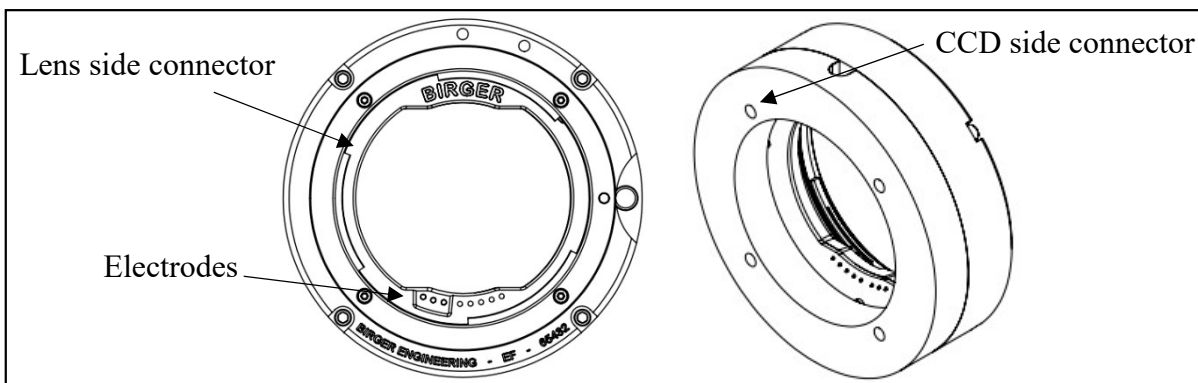


Figure 2: Birger Engineering focus rings (Birger Engineering, Inc. 2017).

connection between the lenses' circuitry and a control computer. By connecting to the circuitry of the lens, the computer is able to automatically control the focus of the lens.

2.3 CCD cameras

The cameras used for this project are Aluma 3200 CCD cameras from Diffraction Limited. With a pixel size of $6.8 \mu\text{m}$ and an imaging array of 2184 pixels by 1472 pixels, the Aluma cameras provide a sizable $2.13^\circ \times 1.43^\circ$ field of view (Diffraction Limited 2018). The Aluma 3200 also has a great peak quantum efficiency of nearly 90% (Diffraction Limited 2018).

2.4 Mac Mini

The control computer for QuAIL is the 2018 Apple Mac Mini. The Mac Mini is a small but powerful computer with 3.2 GHz CPU, a 1 TB solid state drive, and 32 GB of RAM. The Mini has four Thunderbolt 3 ports, two USB 3.0 ports, and an HDMI 2.0 port. The HDMI port will be used to run the monitor and the USB ports will be used to run the keyboard and mouse. As the remaining ports are Thunderbolt 3, Thunderbolt 3 to USB 3.0 adapters will be used to connect to the focus rings and CCD cameras.

2.5 Lens cages

The lens cages are large metal tubes in which the Canon lenses are mounted. The exterior surface of the tubes is hexagonal to allow the tubes to be arranged in a honeycomb pattern (Figure 3 below). This lens mounting system was originally designed by CreateTech Enterprises

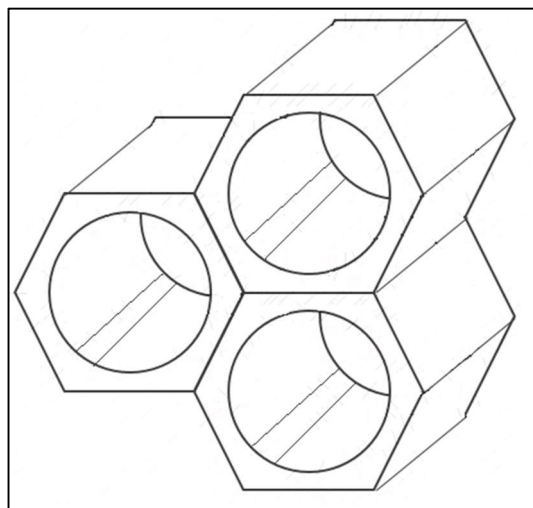


Figure 3: Diagram of lens cages in example configuration. Diagram by Author.

Inc. in Arizona for use in the Dragonfly project. Create Tech was able to supply QuAIL with the same lens cages as were made for Dragonfly.

2.6 Filters

Acquiring the filters required for this project proved to be a particularly difficult task. To avoid the cost of making large filters to cover the front of the Canon lenses it was decided that the filters should be made small enough to place in each lens's 52 mm drop-in filter slot. The filters would thus need to be 49 mm in diameter, placed in a 52 mm screw-in filter frame to attach to the drop-in filter holder. To maximally isolate line emission, they were specified to allow a wavelength range of only 1.0 nm through when exposed to an $f/2.8$ beam of light. The $f/2.8$ was the main source of the difficulty: the half-cone angle of an $f/2.8$ beam is 10.1° and, according to CVI Laser Optics, at an angle of only 5° an interference filter with a full-width half-maximum (FWHM) of 1.0 nm would transmit over 90% less light than it originally could. Additionally, if we assume the refractive index of the filter to be even the typical 1.5 of glass, then $H\alpha$ radiation entering the filter at the half-cone angle would be shifted from 656.28 nm to 651.78 nm, a wavelength change almost five times the bandwidth of the filter. Consequently, the transmission curve is broadened.

Another complication in the designing of the filters stemmed from the need to isolate the target galaxy's $H\alpha$ spectral line from any Milky Way radiation along the line of sight. The two primary potential targets, And XVIII and And XVI, have heliocentric radial velocities of -332.1 km/s and -385.0 km/s respectively, so their respective blue-shifted $H\alpha$ wavelengths are 655.55 nm and 655.44 nm (Tollerud et al. 2012; McConnachie 2012). To build a 1.0 nm $H\alpha$ filter to observe these two galaxies without interference from the Milky Way's $H\alpha$ line, the filter would not only have to have at least three cavities, ideally four, but it would also be necessary to center the filter not on 655.55 nm but on 655.28 nm. A three-cavity filter has a full-width of 2 nm at the point where the filter's transmission has fallen to 1% of its peak value (the "1% point") so the peak of the Milky Way's $H\alpha$ radiation at 656.28 nm would lie just on the 1% point of a 1.0 nm filter if it is centered at 655.28 nm and has three cavities.

Another issue in filter selection was determining what the minimum peak transmission should be to optimize the exposure time. For this purpose a "figure of merit" (FM) was defined where the FM is equal to the peak transmission divided by the filter's equivalent width.

Assuming a Gaussian transmission curve, the equivalent width is 1.06 times the FWHM. In this way, doubling the FM means reducing the required exposure time by half, which is achieved by increasing the transmission or by decreasing the width (admitting less continuum). Calculations were done to determine the exposure time required to collect enough light to effectively observe a very-low surface brightness galaxy. As the exposure calculations involved nearly 50 inputs they were done in Microsoft Excel. From these calculations it was determined that a sufficiently short exposure time was provided, given a FWHM of 1.0 nm, with a FM of 0.66, thus a peak transmission of 0.7, although a greater peak transmission is highly desirable. A target with an H α flux of 1.0×10^{-18} erg/s/cm²/arcsec² would have an equivalent H α surface brightness of approximately 26 mag/arcsec². Given a sky surface brightness of approximately 18 mag/arcsec² at York University and a 1.0 nm wide filter with 90% peak transmission, it would require approximately 537,000 seconds (~18.7 days) of observation to obtain a sufficient image of the target. Using the same filter at a dark sky site with sky surface brightness of 21 mag/arcsec², the exposure time required would be reduced to approximately 34,600 seconds (~1.20 days).

Many filter manufacturers were contacted for their input on how to make the filters but only one was found to be capable: Materion. By designing an original filter system reminiscent of a sandwich, Materion is able to produce a filter utilizing high-index glass on either side of the coating which accepts an *f*/2.8 beam and transforms it to an *f*/5 beam which passes through the coating, then transforms the beam again so that it exits as *f*/2.8 (Shnapir 2019). The transmission curve for a 1.0 nm filter of this design indicates that at the 1% point, the transmission band only increases to ± 1.1 nm (Shnapir 2019). This means that a filter centered on 655.28 nm would collect only a little more than 1% of any light from the Milky Way's 656.28 nm H α line had the filter been centered on that line. This is, of course, assuming that the Milky Way is emitting H α in our chosen direction. From neutral hydrogen surveys, we know that there is Milky Way neutral gas along the line of sight to And XVIII and And XVI but this does not necessarily mean that it is emitting in H α . The Materion filters would also be exceptionally insensitive to temperature changes; Boris Shnapir of Materion has indicated that these filters would experience a shift of only 0.005 nm/°C (Shnapir 2019).

The final obstacle to overcome in acquiring filters ended up being the price. Filters of 49 mm diameter made to the specifications provided by Materion would cost upwards of \$14,000

(USD) per filter, far out of the price range affordable for this project (Shnapir 2019). However, it was determined that the special high refractive index glass used to meet the filter specifications was the driving force in the filter price. Thus, it was decided to reduce filter size to a diameter of 25 mm. Instead of placing filters in the drop-in filter holder of the lenses, they would be mounted directly in front of the CCD. In this way the filter price was able to be reduced to within the project budget. Although the filters have yet to be ordered at the time of writing this will be done in the near future. An additional savings may be possible if filters can be tilted slightly to accommodate targets with different velocities.

3 Software

3.1 Autoguider control

As this project involves taking extremely long exposures software had to be developed to provide autoguiding. With York University's current observatory control program, "DomeTracker", unguided exposures are possible for exposure times up to one minute in length. However, QuAIL will require exposures as long as 15 to 20 minutes each. Protocols thus had to be created and integrated into DomeTracker to check if the field of view was drifting and, if it found that it was, determine how large of a shift had occurred then instruct the telescope to correct its position by this amount. In order to do this, programs had to be developed which could 1) measure the shift in field of view and 2) directly control the telescope's CCD camera through Python.¹

The Python program developed to measure the field of view shift between two images is named "*donutstest.py*." This program is dependent on a Python module called "Donuts" designed by James McCormac and Simon Walker of the University of Warwick (McCormac et al. 2013). The Donuts function accepts an input of two *.fits* images, one called the "reference image" and the other the "science image," and maps out all of the stars found in the reference image then computes the difference in pixel position between the stars in the two images, returning the number of pixels plus direction shifted in the x and y planes (McCormac et al. 2013). The *donutstest.py* program uses Donuts to determine if the telescope has drifted too far, compared to a pre-set drift maximum, and instructs DomeTracker to re-align if it has.

¹ Code for DomeTracker with the new protocols available at: <https://github.com/KatherineGolden/QUAIL>

To be able to communicate with the CCD camera through Python it was necessary to interact directly with the CCD's driver file. As the driver file for the CCD was written in the C programming language this was not an easy task. Matthew Cutone, a highly experienced programmer, was consulted. Matthew aided in the creation of the file named "*libsbig.py*" which is able to read in the driver functions from the driver library. This file contains all of the function definitions required for controlling the CCD camera, such as functions to set a desired "setpoint temperature" and instruct the CCD to cool down to this temperature, and functions to open the CCD's shutter and take an exposure. The *libsbig.py* program interacts with a file called "*imageNumberFile.txt*" to determine how many exposures have previously been taken so that new images can be named appropriately as well as a file called "*ccdconfig.txt*", a configuration file, to determine the user-set values such as exposure length, setpoint temperature, etc.

The new protocols developed for DomeTracker call on *libsbig.py* to cool the CCD to the setpoint temperature, take exposures, and determine the current CCD's configuration. They also call on *donutstest.py* periodically throughout an observing session to determine if a shift is necessary. Additionally, at the beginning of each night, the new protocols use *donutstest.py* to recalibrate the telescope so as to adjust for wear to the telescope's gears which may occur over long periods of time and cause the telescope to move faster or slower. The configuration process procedure, outlined in Appendix 1, involves moving the telescope North, South, East, and West whilst taking pictures and comparing the shift in pixels caused by each move (Figure 4 below).

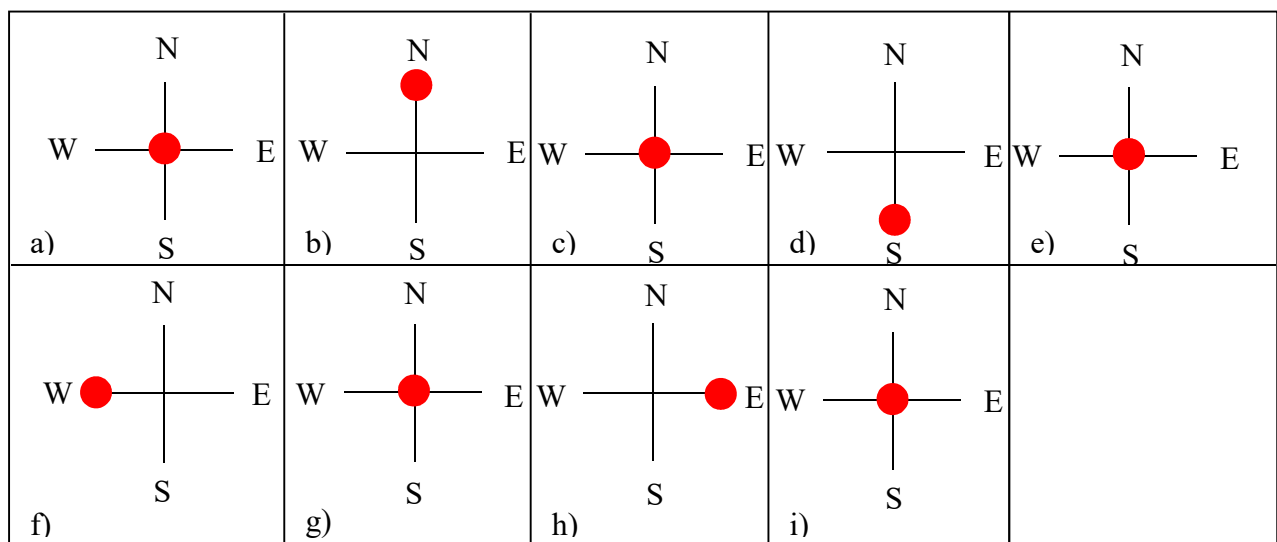


Figure 4: Motion path of the telescope (represented by the red dot) during calibration. The telescope starts at the origin (a) and moves North/South/East/West through the positions (a) to (i). Diagram by Author.

After running the configuration protocols, DomeTracker knows the number of pixels per step at a specified speed as well as the number of pixels per arcsecond as seen by the CCD. With the new protocols, DomeTracker can then proceed with several hours of observation with little to no further input from the user. The new DomeTracker protocols were integrated with the main program, *DomeTrackerApp.py*, by Anna Skrinnik.

3.2 QuAIL control

The Dragonfly group has used GitHub to provide public access to the code they designed for their project.² The Dragonfly code, written primarily in C and Perl, was designed to control Dragonfly's CCD cameras and Birger focus rings as well as various other observatory systems and devices they required for observing sessions (Abraham & van Dokkum 2013). The scripts used for CCD and focus ring control will be adapted in the future for use by QuAIL to control the Aluma 3200 CCDs and the focus rings.

4 Testing and Results

Various tests were performed on the Canon lenses to determine how they could best be used for QuAIL. Several tests were done which did not end up being useful or necessary, such as determining the beam size at the location of the drop-in filter holder (See Appendix 2). For tests whose results proved fruitful, the tests and their results have been explained below.

4.1 Field of view

It was important to determine the field of view of the lens to know how far off the side of the 60 cm telescope QuAIL had to be mounted. To examine the field of view, the lens was mounted in one of the lens cages and connected to a Canon camera. A meter stick was placed vertically against a wall and a picture was taken. By measuring the distance from the front of the lens to the target as well as the distance from one edge of the image to the other, the angle of the field of view was able to be calculated. From the small resultant angle it was clear that the end of the 60 cm telescope barrel would be well outside the field of view. As the Aluma 3200 CCD results in a much smaller field of view than the Canon camera, it was determined that QuAIL could be mounted directly against the side of the 60 cm telescope and the telescope barrel would

² Dragonfly code available at: <https://github.com/robertoabraham/ProjectDragonfly>

still be far outside the field of view. The optical system created by using the Aluma 3200 with the Canon lens had a field of view of 2.13° (127.6 arcmin) by 1.43° (86.0 arcmin).

4.2 Optical path flexibility

It was important to determine the feasibility of increasing the distance between the lens and the CCD camera to know if it would be possible to add a filter holder or filter wheel between the lens and the CCD in the future, as well as to determine if it was possible to use a filter with a different refractive index and/or thickness than the clear ‘faux-filter’ that came with the lens. These questions were first tackled using matrix optics (See Appendix 3) then the results were verified experimentally by using first the faux-filter and adjusting the focus of the lens then repeating the process using a filter with a higher index of refraction.

The relationship between filter thickness, filter refractive index, and distance between filter and camera is given by

$$x_i + d_i/n_i = x_f + d_f/n_f = \text{const.},$$

where x is the distance between the filter and the camera, d is the thickness of the filter, and n is the refractive index of the filter. Subscript i indicates initial values and subscript f indicates new values. From this relationship it is found that a filter with a higher index of refraction than the faux-filter, which will be required, would mean that the distance between the CCD and the filter would have to be increased or the filter thickness decreased.

Through the lens testing with the alternate filter it was determined that a change in index of refraction or in filter thickness was able to be overcome by simply adjusting the focus of the lens. Filter-to-CCD distance, filter thickness, and filter index of refraction are therefore all able to be adjusted independently.

5 Sample Selection

Sample selection began by looking through Karachentsev’s *Updated Nearby Galaxy Catalog* (Karachentsev et al. 2013). Potential targets needed to be dwarf spheroidal galaxies which were: 1) sufficiently dim; 2) not likely to have had their gas stripped away by a nearby galaxy; 3) have known velocities; and 4) would be visible in the night sky during the spring, which was the projected observing season. The target group was subsequently expanded to include galaxies visible at other times of the year.

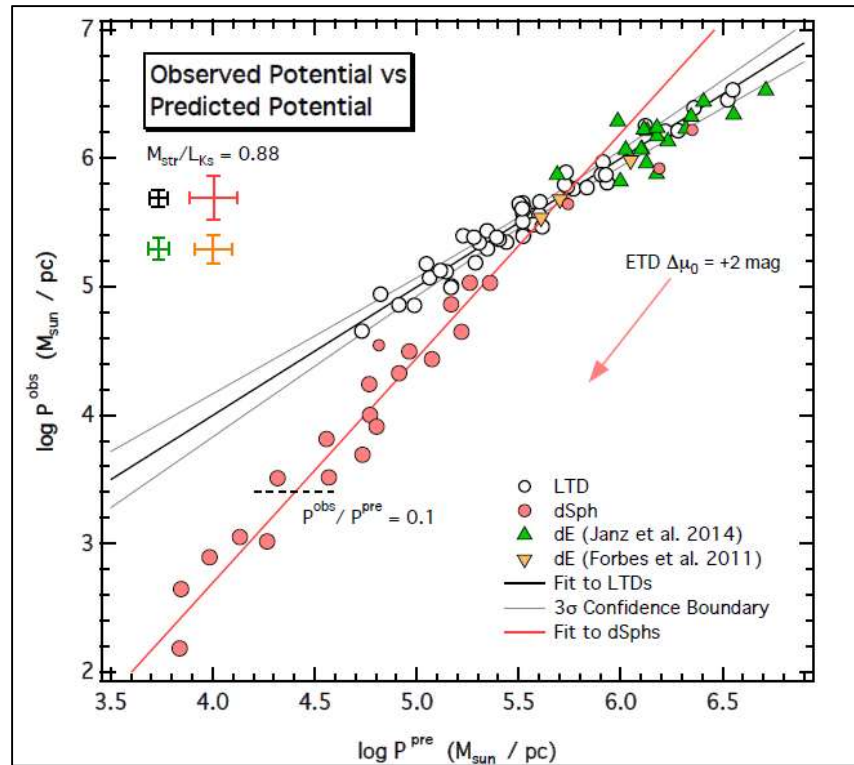


Figure 5: Observed potential vs predicted potential for dwarf galaxies. The Potential Plane (black solid line) is the fit to late-type dwarfs. Dwarf spheroidals lie below the plane, likely because of gas lost. Adapted from Ivkovich and McCall (2019).

The “potential plane” is defined by the relationship between the observed potential from baryonic mass and radius of LTDs and their predicted potential from internal motions and surface brightness (Ivkovich & McCall 2019). In Figure 5 (above), it can be seen that dSphs fall below the potential plane detailed by dEs for values of $\log P^{\text{pre}}$ lower than approximately 5.5. This implies that the smaller dSphs have lower than expected mass, perhaps caused by a depletion of gas. In Figure 6 (below), one finds that dwarf galaxies with $\log P^{\text{pre}} \sim 5.5$ have an absolute magnitude in K of approximately -16.5. It is thus clear that dSph galaxies with absolute K magnitudes fainter than -16.5, which is -13.4 in B, are likely to have lost mass due to some process. To ensure that potential targets have lost a notable fraction of their mass, all galaxies with absolute magnitude in K brighter than -15.0 were excluded. A list was thus compiled of all dSph galaxies in Karachentsev’s catalog with an absolute B magnitude fainter than -11.9.

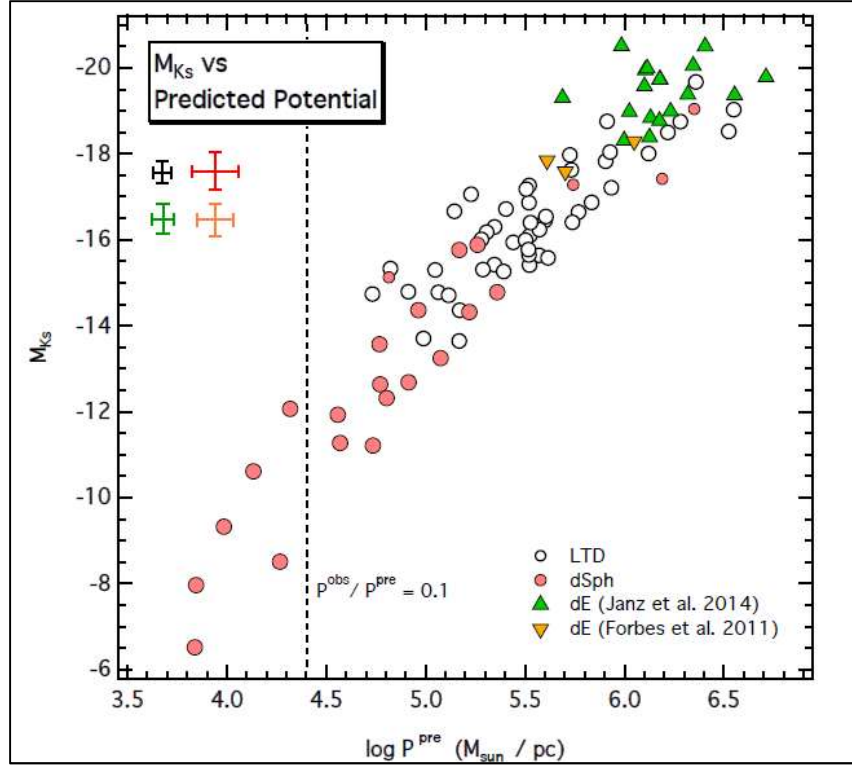


Figure 6: Predicted potential vs absolute magnitude in K for dwarf galaxies. Dashed line marks the value of $\log P^{\text{pre}}$ at which dSphs are believed to contain only 10% of their original total baryonic mass. Adapted from McCall (2019).

As the goal of this project was to look for evidence of gas loss which was not caused by galaxy interactions, it was necessary to identify dSphs far enough away from other galaxies, particularly the more massive galaxies, that they were unlikely to have lost gas through processes like ram pressure or tidal forces. Karachentsev describes the gravitational environment around a galaxy by a value called the “tidal index” (Karachentsev et al. 2013). Karachentsev et al. (2013) compute the tidal force magnitude, F_{TFM} , between each cataloged galaxy and its neighbours “ n ” using the formula $F_n \sim \frac{M_n}{D_{in}^3}$, where D_{in} is the distance between the galaxy and its neighbour and M_n is the neighbouring galaxy’s mass. The tidal index, Θ , of the galaxy’s most gravitationally significant neighbour (that which has the highest F_{TFM} , called the “main disturber” or “MD”) is then computed as

$$\Theta = \max \left[\log \left(\frac{M_n}{D_{in}^3} \right) \right] + C, \quad n = 1, 2, \dots, N,$$

where the constant, C , was picked as having a value of -10.96 (Karachentsev et al. 2013). The value of C was chosen so that at $\Theta = 0$ a target galaxy lies on the zero velocity sphere relative to its MD (Karachentsev et al. 2013). Galaxies with $\Theta > 0$ are therefore members of a certain group

while negative values of Θ correspond to isolated galaxies (Karachentsev et al. 2013). For the purposes of this project, galaxies were initially deemed to be far enough away from their MD if they had tidal indices of 1.0 or less rather than only if they had a negative tidal index as dSphs tend to be found near other galaxies. After removing galaxies with tidal indices greater than 1.0 only one potential spring target remained which also had a known heliocentric radial velocity: KK180. It is important that the heliocentric radial velocity of a target is known when observing with narrow band filters as the central wavelength of the filter must be adjusted for the Doppler shift in spectral lines caused by this motion. Upon further research into KK180, it was discovered that Makarov et al. (2015) measured a new distance to this galaxy much greater than previously believed, so the true absolute magnitude of KK180 is far too bright for it to be a viable dSph candidate. Having exhausted the list of potential spring targets with these criteria, the decision was made to increase the isolation criterion to a maximum tidal index of 2.0 with special interest given to galaxies with an index of 1.5 or lower. This decision was made alongside the realization that few dSph galaxies would be found with what had previously been deemed as a low enough isolation criterion as they are preferentially located near massive galaxies. After relaxing the criterion, several potential spring targets were discovered. One of the more promising potential targets on the spring list at this point, DDO 078, had to be excluded due to the presence of a very bright star too close to the galaxy in the CCD's field of view.

At this point it became unclear if using the original observing window, the spring, would be possible so the search for targets was expanded to include fall objects. When the list of potential fall targets was completed, it was clear that there was a strong front runner: And XVIII. The galaxy And XVIII has a low tidal index of 0.4 and, since it is a satellite of Andromeda, it is near enough that it should be easily visible in the sky even though it is a small, dim galaxy. Additionally, another potential fall target, And XVI, is moving with a heliocentric radial velocity close enough to that of And XVIII for both to be studied using the same narrow band filter.

To ensure that there would be no ionized gas from the Milky Way interfering with the view of the target galaxies, a neutral hydrogen velocity map was consulted: the HI4PI full-sky HI survey (Bekhti et al. 2016). For the northern hemisphere, the HI4PI survey provides the intensity of HI at velocities between -600 km/s and +600 km/s in FITS data cubes which can be searched by right ascension and declination (Bekhti et al. 2016). As the process for extracting the velocity

vs intensity data points was extremely time consuming, taking up to half an hour for each target, this process was only done for the most promising potential targets. The velocities of the potential target galaxies, in the heliocentric frame, were converted to the local standard of rest velocity frame to compare to the neutral hydrogen velocity. This was done with the assumption that Milky Way gas in any other form would be moving with the same velocity as the neutral hydrogen. Several potential spring and fall targets, including And XVIII and And XVI, were found to be moving with sufficient speed for their H α lines to be isolated from Milky Way spectral lines.

The final set of potential targets for spring can be found in Appendix 4 and for fall in Appendix 5. For the galaxies for which they were collected, galaxy images and HI spectra, with V_{LSR} in m/s, can be found in Appendix 6.

6 Future Plans

Starting in September 2019, Anna Skrinnik will be switching from working on the QuAIL project in a secondary capacity to being the lead grad student for the project. In the near future, Anna will finalize the autoguiding code to optimize the observing procedures. Additionally, the Dragonfly code will be adapted by Anna for use as the QuAIL control code. Anna will also implement a plan for data analysis, likely including cloud computing.

Once the control codes have been finalized, mainly through running observational trials and adjusting the code to work out any bugs in the observational procedures, observing can begin on campus. Initially, the narrow-band H α filters will be used to look for ionized hydrogen around the target galaxies. Additional narrow band filters, particularly one for the [O I] 636.4 nm line, may be acquired to look for spectral evidence of shock waves. Additionally, future observing may be done off campus with QuAIL at a dark sky site.

7 Conclusions

The QuAIL project seeks to build off the work done by the Dragonfly group, utilising an array of Canon EF 400 mm $f/2.8$ L IS II USM telephoto lenses connected to Aluma 3200 CCD cameras to create an optical system with an effective lens speed much faster than possible with a single telescope. Unlike the Dragonfly array, QuAIL will take this superb light collection system and use it with narrow-band filters to eliminate pollution from light at other wavelengths. In doing this QuAIL will be able to study emission lines from ultra-low surface brightness galaxies.

The foundations of the QuAIL project have been set and the project is now ready to move forward and attempt to answer some of the puzzling questions about the elusive ultra-low surface brightness universe.

References

- Abraham, R. G., and van Dokkum, P. G., 2013, *PASP*, 126, 55.
- Bekhti, N. B., Flöer, L., Keller, R., Kerp, J., Lenz, D., Winkel, B., ... and Staveley-Smith, L., 2016, *AA*, 594, 116.
- Birger Engineering, Inc., 2017, *Birger Canon EF Adapter for SBIG Camera*. <https://birger.com/products/rd/rd-ef1-sb0-x.pdf>.
- Boissier, S., Boselli, A., Ferrarese, L., Côté, P., Roehly, Y., Gwyn, S. D. J., ... and Madore, B. F., 2016, *AA*, 593, 126.
- Carnathan, B., 2011, *Canon EF 400mm f/2.8L IS II USM Lens Review*. <https://www.the-digital-picture.com/Reviews/Canon-EF-400mm-f-2.8-L-IS-II-USM-Lens-Review.aspx>.
- CVI Laser Optics, Interference Filter Coatings, *CVI Melles Griot Technical Guide*, Volume 2, Issue 2.
- Diffraction Limited, 2018, Aluma 3200: Specifications. <http://diffractionlimited.com/product/aluma-3200/>.
- Ivkovich, N., and McCall, M., 2019, *MNRAS*, 486, 2, 1964.
- Karachentsev, I. D., Makarov, D. I., and Kaisina, E. I., 2013, *AJ*, 145.
- Kirby, E. N., Cohen, J. G., Guhathakurta, P., Cheng, L., Bullock, J. S., and Gallazzi, A., 2013, *ApJ*, 779, 102.
- Makarov, D. I., Sharina, M. E., Karachentseva, V. E., and Karachentsev, I. D., 2015, *AA*, 581, 82.
- McCall, M., March 7th, 2018, personal communication.
- McCall, M., March 17th, 2019, personal communication.
- McConnachie, A. W., 2012, *ApJ*, 144.
- McCormac, J., Pollacco, D., Skillen, I., Faedi, F., Todd, I., and Watson, C. A., 2013, *PASP*, 125.
- Read, J. I., and Gilmore, G., 2005, *MNRAS*, 356, 1, 107.

Shnapir, B., March 2019, personal communication.

Skiff, B., 1996, *How Dark Can the Night Sky Get?* http://www.astropix.com/html/l_story/skybrite.html#top.

Tollerud, E. J., Beaton, R. L., Geha, M. C., Bullock, J. S., Guhathakurta, P., Kalirai, J. S., ... and Cooper, M. C., 2012, *ApJ*, 752.

Van Dokkum, P. G., Abraham, R., Merritt, A., Zhang, J., Geha, M., and Conroy, C., 2015, *ApJL*, 789.

Appendices

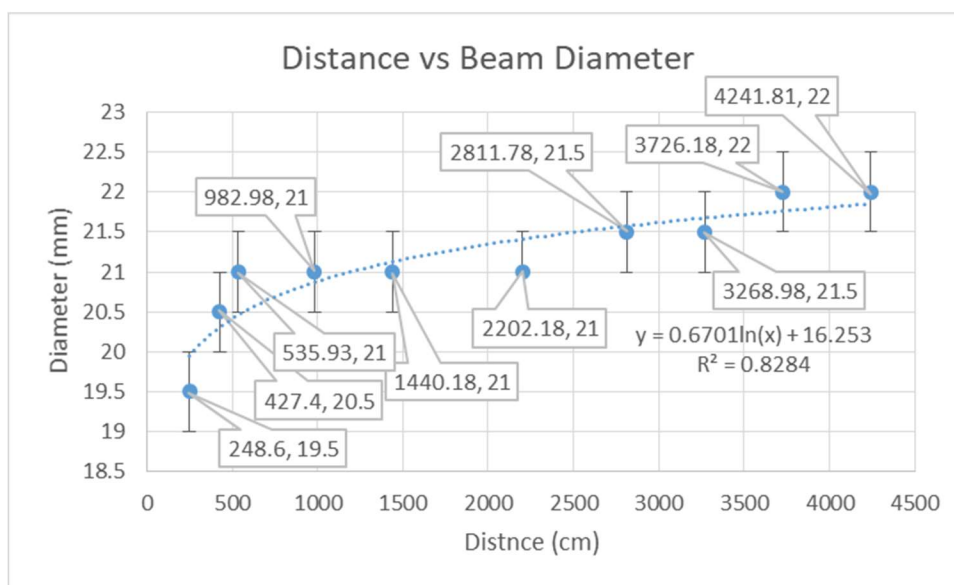
Appendix 1: DomeTracker calibration procedure

- 1) DomeTracker starts at the origin position (Figure 4a)
- 2) DomeTracker calls on *libsbig.py* to take an exposure (Image 1)
- 3) DomeTracker instructs the telescope to move n steps at v speed North (Figure 4b)
- 4) DomeTracker calls on *libsbig.py* to take Image 2
- 5) DomeTracker calls on *donutstest.py* to compare Image 2 to Image 1, Shift 1 is returned
- 6) DomeTracker instructs the telescope to move n steps at v speed South (Figure 4c)
- 7) DomeTracker calls on *libsbig.py* to take Image 3
- 8) DomeTracker calls on *donutstest.py* to compare Image 3 to Image 2, Shift 2 is returned
- 9) DomeTracker instructs the telescope to move n steps at v speed South (Figure 4d)
- 10) DomeTracker calls on *libsbig.py* to take Image 4
- 11) DomeTracker calls on *donutstest.py* to compare Image 4 to Image 3, Shift 3 is returned
- 12) DomeTracker instructs the telescope to move n steps at v speed North (Figure 4e)
- 13) DomeTracker calls on *libsbig.py* to take Image 5
- 14) DomeTracker calls on *donutstest.py* to compare Image 5 to Image 4, Shift 4 is returned
- 15) DomeTracker instructs the telescope to move n steps at v speed West (Figure 4f)
- 16) DomeTracker calls on *libsbig.py* to take Image 6
- 17) DomeTracker calls on *donutstest.py* to compare Image 6 to Image 5, Shift 5 is returned
- 18) DomeTracker instructs the telescope to move n steps at v speed East (Figure 4g)
- 19) DomeTracker calls on *libsbig.py* to take Image 7
- 20) DomeTracker calls on *donutstest.py* to compare Image 7 to Image 6, Shift 6 is returned
- 21) DomeTracker instructs the telescope to move n steps at v speed East (Figure 4h)
- 22) DomeTracker calls on *libsbig.py* to take Image 8
- 23) DomeTracker calls on *donutstest.py* to compare Image 8 to Image 7, Shift 7 is returned
- 24) DomeTracker instructs the telescope to move n steps at v speed West (Figure 4i)
- 25) DomeTracker calls on *libsbig.py* to take Image 9
- 26) DomeTracker calls on *donutstest.py* to compare Image 9 to Image 8, Shift 8 is returned
- 27) DomeTracker averages Shift 1 with Shift 4, Shift 2 with Shift 3, Shift 5 with Shift 8, and Shift 6 with Shift 7. The four averages are saved as NorthResult, SouthResult, WestResult, and EastResult, respectively.
- 28) DomeTracker compares North-, South-, East-, and WestResult with n and v to determine the number of pixels per step at speed v and the number of pixels per arcsecond

Appendix 2: Beam size measurement

At one point in the course of designing filters to accommodate an $f/2.8$ beam, Dr. McCall proposed that a zero-power meniscus filter could be created to fit the beam at the location of the drop-in filter holder. Such a filter would need to have a diameter equal to that of the beam which passes through the filter holder and a radius of curvature such that filter surface is perpendicular to the beam at every point which the beam passes through it.

Tests were performed on the Canon lens to determine the size of the beam at the drop-in filter holder and how this size changes with the distance between the lens and the target. This was done using a Canon camera by bouncing a green laser off a sheet of white paper and focusing the lens-camera system at the location of the reflected laser beam spot. A piece of graph paper was placed inside the filter holder against the clear glass ‘faux-filter’ which came with the lens. The laser beam illuminated the graph paper so that the beam size could be measured when an image was taken. This test was first performed in the laboratory for distances below 536 cm then in the hallway to obtain beam size measurements at distances up to 4242 cm. A graph of the results is provided below with the equation of best fit for the data.



Appendix 3: Matrix optics calculations

Assuming the refractive index of air is equal to 1, n = refractive index of filter, d = filter thickness, x = distance between filter and CCD.

Subscript i indicates original values of the system (lens with ‘faux-filter’, no additional space between lens and CCD), subscript f indicates new values (new filter thickness, new filter refractive index, or new distance between lens and CCD).

$$M_1 = \text{matrix for left side of filter} = \begin{bmatrix} 1 & 0 \\ 0 & \frac{1}{n} \end{bmatrix}$$

$$M_2 = \text{matrix for filter} = \begin{bmatrix} 1 & d \\ 0 & 1 \end{bmatrix}$$

$$M_3 = \text{matrix for right side of filter} = \begin{bmatrix} 1 & 0 \\ 0 & n \end{bmatrix}$$

$$M_4 = \text{matrix for space between filter and CCD} = \begin{bmatrix} 1 & x \\ 0 & 1 \end{bmatrix}$$

$$\therefore M_3 M_2 M_1 = \begin{bmatrix} 1 & \frac{d}{n} \\ 0 & 1 \end{bmatrix} = M'$$

$$\therefore M = M_4 M' = \begin{bmatrix} 1 & x + \frac{d}{n} \\ 0 & 1 \end{bmatrix} = \begin{bmatrix} A & B \\ C & D \end{bmatrix} = \text{matrix of the QuAIL system} \Rightarrow \text{must be maintained}$$

M is the equivalent matrix for the optical system made when the lens, fitted with the clear glass ‘faux-filter’ provided by the lens manufacturer, is connected to the CCD camera via the focus ring. As the optics in this system are those which cause light to be focused on the CCD imaging chip, the elements in the matrix for this system (A , B , C , and D) must remain constant else the light will not be focused on the CCD imaging chip. Therefore, if the distance between the filter and the CCD, the filter thickness, or the refractive index of the filter are changed then at least one of the others must be adjusted accordingly so that the value of B does not change.

$$\therefore B = x + \frac{d}{n} = \text{const.}$$

$$\therefore x_i + \frac{d_i}{n_i} = x_f + \frac{d_f}{n_f}$$

$$\therefore \text{If there is no change in } d \text{ then } \Delta x = d \left(\frac{1}{n_i} - \frac{1}{n_f} \right)$$

$$\text{Let } n_i = n, n_f = n + \Delta n \Rightarrow \Delta x = d \left(\frac{1}{n} - \frac{1}{n + \Delta n} \right)$$

\therefore A filter with a higher index of refraction than the faux-filter requires that the distance between the filter and the CCD be increased.

If n is held constant then $\Delta x = \frac{d_i - d_f}{n} = -\frac{\Delta d}{n}$

∴ If the distance between the CCD and the filter were increased then the filter thickness would have to be decreased, or vice versa.

If x is held constant then $\frac{d_i}{n_i} = \frac{d_f}{n_f} \Rightarrow \frac{d_f}{d_i} = \frac{n_f}{n_i}$

Let $n_i = n, n_f = n + \Delta n$ and $d_i = d, d_f = d + \Delta d$

∴ $\frac{d + \Delta d}{d} = \frac{n + \Delta n}{n} \Rightarrow \frac{\Delta d}{d} = \frac{\Delta n}{n}$

∴ If the distance between the filter and the CCD is to remain constant then any change in filter refractive index would need to be accompanied by an equal *relative* change in filter thickness.

Appendix 4: Spring targets

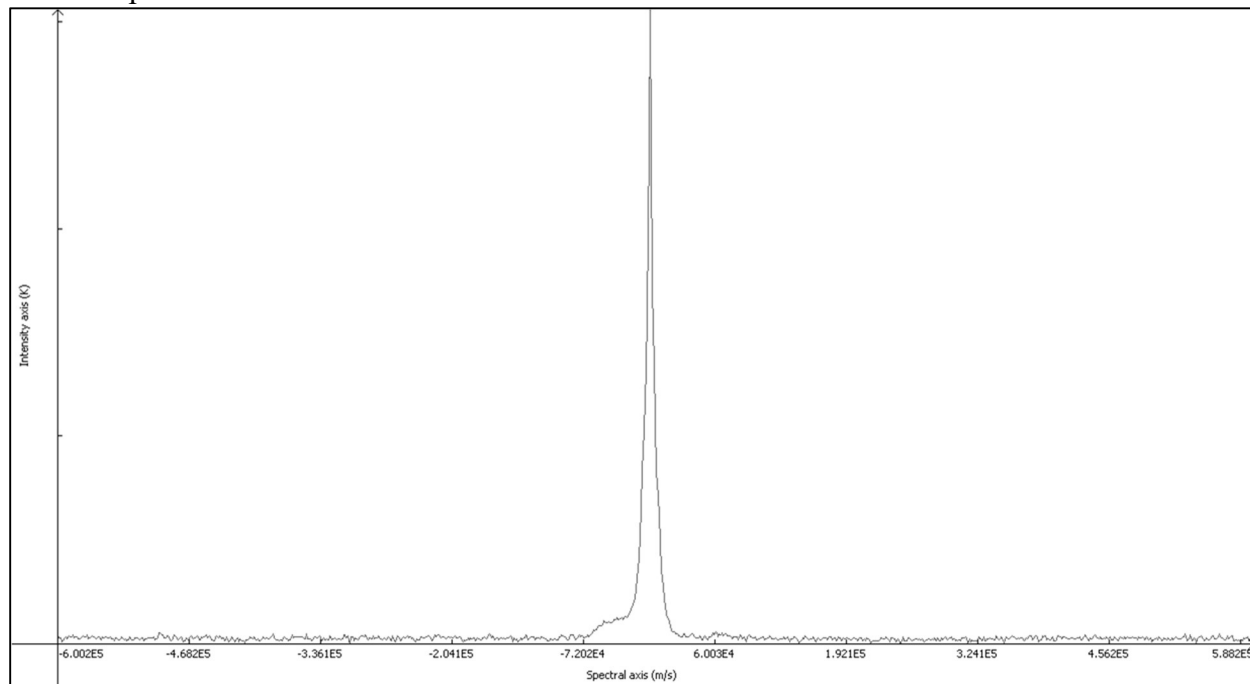
Target name	LeoI	LeoII	CVnI	CVnII
RA (J2000)	10h:08m:26.9s	11h:13m:29.2s	13h:28m:03.5s	12h:57m:10.0s
DEC (J2000)	+12d:18m:29s	+22d:09m:17s	+33d:33m:21s	+34d:19m:15s
V_{\odot} (km/s)	282.5	78.0	30.9	-128.9
V_{LSR} (km/s)	277.2	78.4	40.7	-120.9
H α λ (nm)	656.90	656.45	656.35	656.00
M_{B}	-11.0	-9.1	-7.9	-4.1
M_{V}	-11.6	-9.7	-8.5	-4.7
M_{K}	-14.1	-12.2	-11.0	-7.2
Tidal index	1.4	1.6	1.5	2.0
Distance (Mpc)	0.25	0.21	0.22	0.16

Appendix 5: Fall targets

Target name	And II	And XVIII	And XIX	And XVI	And XXIV
RA (J2000)	01h:16m:29.8s	00h:02m:14.5s	00h:19m:32.1s	00h:59m:29.8s	01h:18m:30.0s
DEC (J2000)	+33d:25m:09s	+45d:05m:20s	+35d:02m:37s	+32d:22m:36s	+46d:21m:58s
V_{\odot} (km/s)	-194.0	-332.1	-111.0	-385.0	-128.0
V_{LSR} (km/s)	-195.3	-327.8	-108.8	-385.5	-127.3
H α λ (nm)	655.86	655.55	656.04	655.44	656.00
M_{B}	-9.2	-9.1	-8.3	-8.2	-7.0
M_{V}	-9.8	-9.7	-8.9	-8.8	-7.6
M_{K}	-12.3	-12.2	-11.4	-11.3	-10.1
Tidal index	2.0	0.4	1.9	1.5	1.9
Distance (Mpc)	0.65	1.36	0.93	0.52	0.6

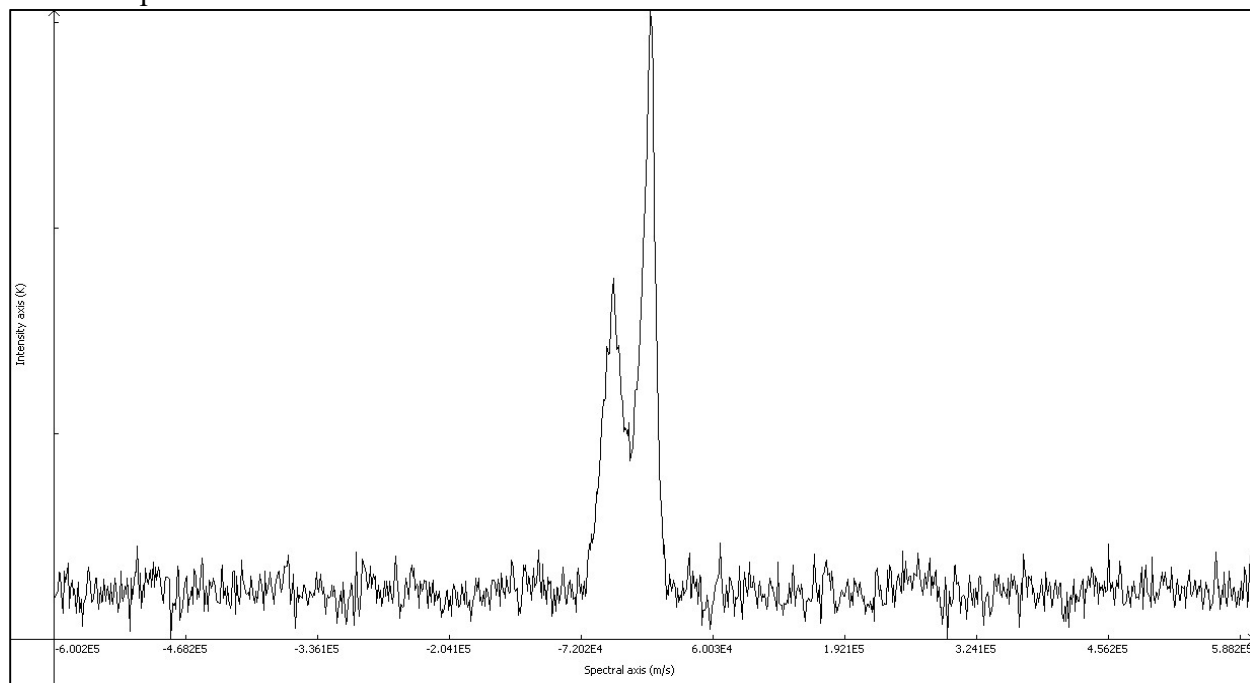
Appendix 6: HI spectra and galaxy images

LeoI HI spectrum:



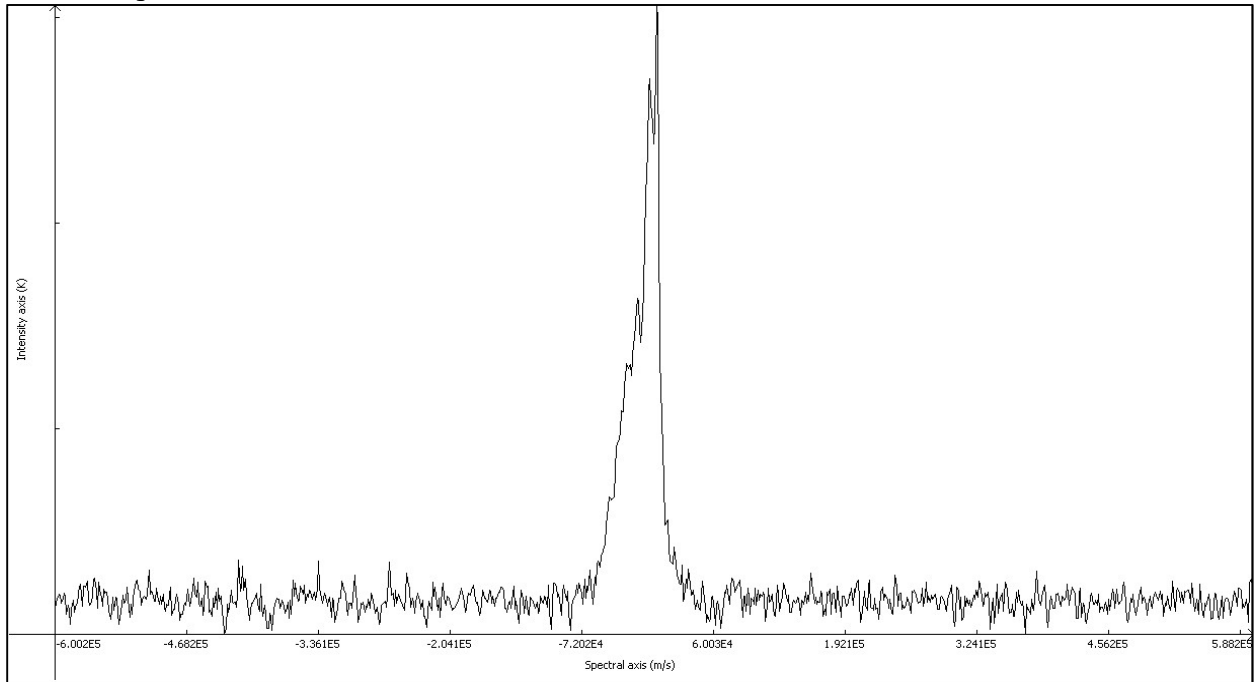
(Maximum intensity of 15.30 K at V_{LSR} of -5052 m/s)

LeoII HI spectrum:



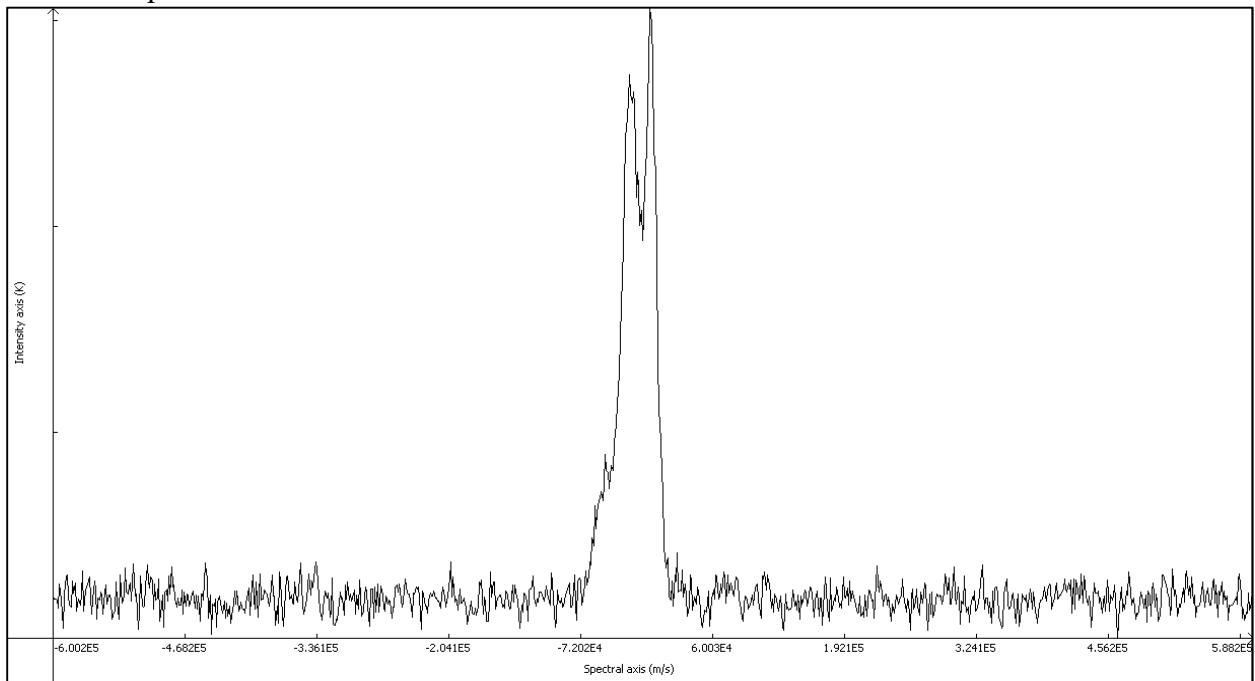
(Maximum intensity of 1.40 K at V_{LSR} of -2946 m/s)

CVnI HI spectrum:



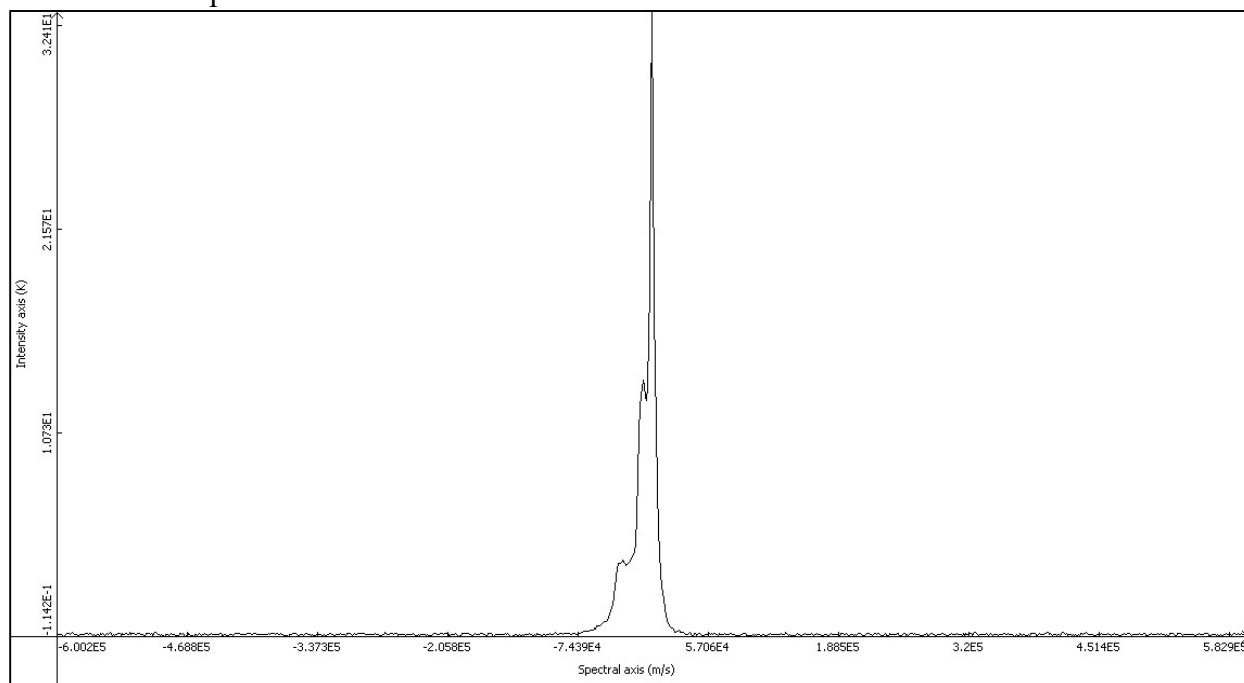
(Maximum intensity of 1.80 K at V_{LSR} of +2677 m/s)

CVnII HI spectrum:



(Maximum intensity of 1.34 K at V_{LSR} of -2475 m/s)

And XVIII HI spectrum:



(Maximum intensity of 20.10 K at V_{LSR} of +14271 m/s)

And XVIII image:

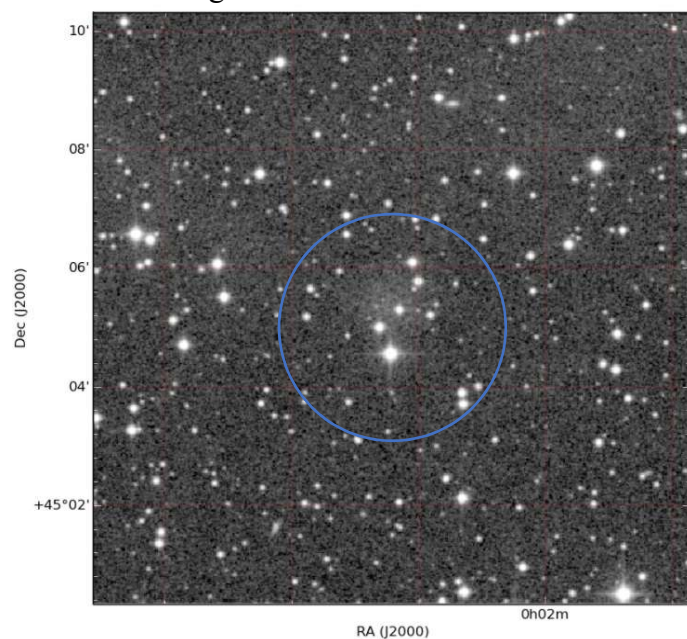
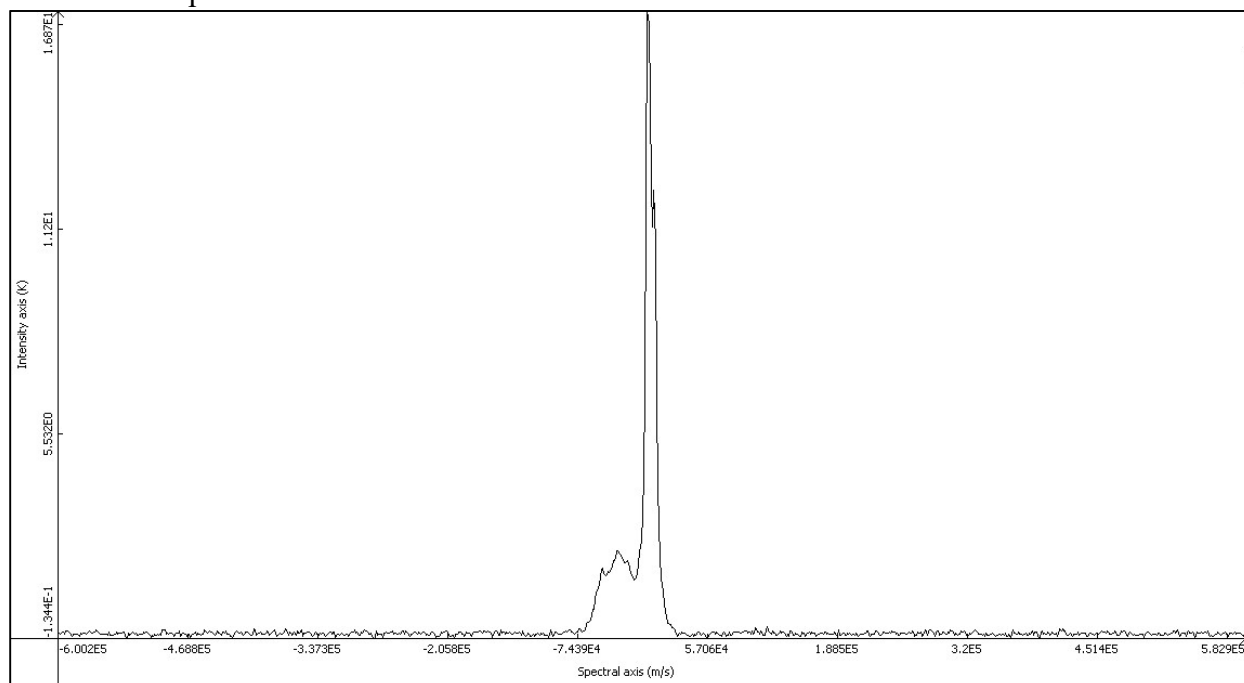


(Image from POSS-II F Red (XP) survey, galaxy circled in blue)

And XVI HI spectrum:



(Maximum intensity of 13.76 K at V_{LSR} of +14271 m/s)

And XVI image:

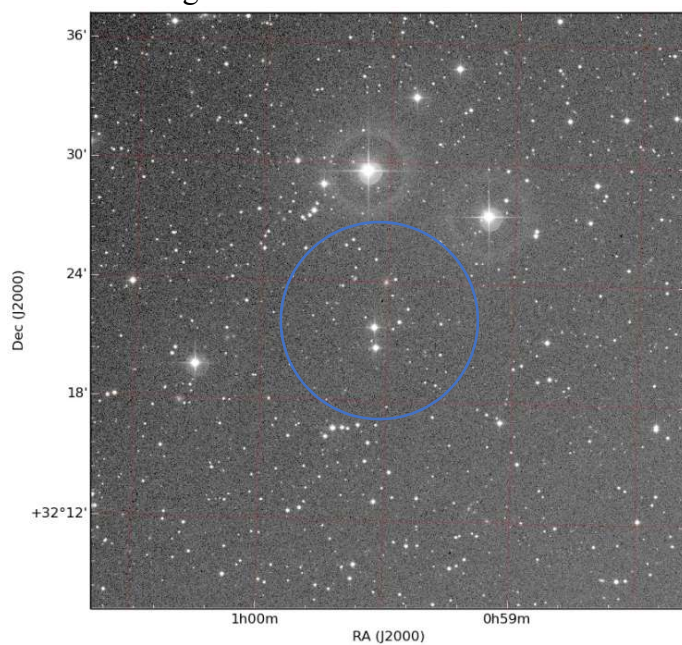


(Image from POSS-II F Red (XP) survey, galaxy circled in blue)